BIOMOLECULES
& THERAPEUTICS

Picropodophyllotoxin Inhibits Cell Growth and Induces Apoptosis in Gefitinib-Resistant Non-Small Lung Cancer Cells by Dual-Targeting EGFR and MET

Jin-Young Lee[1,†], Bok Yun Kang[2,†], Sang-Jin Jung[3], Ah-Won Kwak[3], Seung-On Lee[4], Jin Woo Park[3,4], Sang Hoon Joo[5], Goo Yoon[3], Mee-Hyun Lee[6,]* and Jung-Hyun Shim[3,4,7,]*

[1]Department of Biological Sciences, Keimyung University, Daegu 42601,
[2]College of Pharmacy, Chonnam National University, Gwangju 61186,
[3]Department of Pharmacy, College of Pharmacy, Mokpo National University, Muan 58554,
[4]Department of Biomedicine, Health & Life Convergence Sciences, BK21 Four, College of Pharmacy, Mokpo National University, Muan 58554,
[5]College of Pharmacy, Daegu Catholic University, Gyeongsan 38430,
[6]College of Korean Medicine, Dongshin University, Naju 58245, Republic of Korea
[7]The China-US (Henan) Hormel Cancer Institute, Zhengzhou, Henan 450008, China

Abstract

Patients with non-small-cell lung cancer (NSCLC) with epidermal growth factor receptor (EGFR) amplification or sensitive mutations initially respond to the tyrosine kinase inhibitor gefitinib, however, the treatment becomes less effective over time by resistance mechanism including mesenchymal-epithelial transition (MET) overexpression. A therapeutic strategy targeting MET and EGFR may be a means to overcoming resistance to gefitinib. In the present study, we found that picropodophyllotoxin (PPT), derived from the roots of *Podophyllum hexandrum*, inhibited both EGFR and MET in NSCLC cells. The antitumor efficacy of PPT in gefitinib-resistant NSCLC cells (HCC827GR), was confirmed by suppression of cell proliferation and anchorage-independent colony growth. In the targeting of EGFR and MET, PPT bound with EGFR and MET, *ex vivo*, and blocked both kinases activity. The binding sites between PPT and EGFR or MET in the computational docking model were predicted at Gly772/Met769 and Arg1086/Tyr1230 of each ATP-binding pocket, respectively. PPT treatment of HCC827GR cells increased the number of annexin V-positive and subG1 cells. PPT also caused G2/M cell-cycle arrest together with related protein regulation. The inhibition of EGFR and MET by PPT treatment led to decreases in the phosphorylation of the downstream-proteins, AKT and ERK. In addition, PPT induced reactive oxygen species (ROS) production and GRP78, CHOP, DR5, and DR4 expression, mitochondrial dysfunction, and regulated involving signal-proteins. Taken together, PPT alleviated gefitinib-resistant NSCLC cell growth and induced apoptosis by reducing EGFR and MET activity. Therefore, our results suggest that PPT can be a promising therapeutic agent for gefitinib-resistant NSCLC.

Key Words: Picropodophyllotoxin (PPT), EGFR, MET, Non-small cell lung cancer, Apoptosis

INTRODUCTION

Picropodophyllotoxin (PPT) is an epimer of podophyllotoxin (PT), which is a bitter-tasting aryltetralin-type lignan and was the main component in the alcohol-soluble fraction of *Podophyllum* species (Canel *et al*., 2000; Gordaliza *et al*., 2004;

Shah *et al*., 2021). PT targets microtubule assembly and exhibits potent anticancer activity but has severe systemic toxicity in normal cells (Gordaliza *et al*., 2004; Zhao *et al*., 2021). Thus, PPT with a low toxicity, 50% lethal dose (LD$_{50}$) of more than 500 mg/kg in rodents was developed (Girnita *et al*., 2004; Vasilcanu *et al*., 2004). Interestingly, despite its high structural

---

www.biomolther.org

similarity, PPT did not decrease tubulin assembly or topoisomerase activity, unlike PT, but it inhibited insulin-like growth factor-1 receptor activity (Girnita et al., 2004). Recently, PPT was reported to exert anticancer effects in colorectal cancer and esophageal squamous cell carcinoma by inducing apoptosis via ROS-induced Jun N-terminal kinase/p38 mitogen-activated protein kinase pathways (Kwak et al., 2020; Lee et al., 2021). However, the molecular mechanism of PPT involved in anticancer activity has not been completely elucidated.

Lung cancer is the first leading cause of cancer-related deaths worldwide in both males and females excluding gender-specific cancers (International Agency for Research on Cancer, 2020). It is estimated to cause 68,820 deaths in males and 61,360 in women in the United States (US) in 2022, with more than 80% attributed to smoking (Siegel et al., 2022). And the number of people surviving since a diagnosis on January 1, 2022, in the US was estimated at 287,050 and 367,570 for males and females, respectively (Miller et al., 2022). Lung cancer treatment differs according to the classification, in which ~14% are small-cell lung cancer (SCLC) and ~82% are non-small cell lung cancer (NSCLC) (Griffin and Ramirez, 2017; Miller et al., 2022). In genome-associated targets, the major causes of lung cancer are known to be epidermal growth factor receptor (EGFR) mutation, mesenchymal-epithelial transition (MET) amplification and anaplastic lymphoma kinase translocation, and Kirsten rat sarcoma viral oncogene mutation (Akhtar and Bansal, 2017; Griffin and Ramirez, 2017; Tian et al., 2022).

EGFR mutations in NSCLC account for 10-15% of adenocarcinoma in white patients and ~50% in Asians (Engelman and Janne, 2008; Kosaka et al., 2011; Shah and Lester, 2020). These findings suggest that EGFR mutation activates related signaling pathways, thus inducing lung cancer growth and progression. Gefitinib, a receptor tyrosine kinase inhibitor, is an EGFR-targeted inhibitor to which lung cancer patients with EGFR mutations respond (Kris et al., 2003; Kosaka et al., 2011). However, resistance emerges within six months after therapy (Engelman and Janne, 2008; Kosaka et al., 2011; Brugger and Thomas, 2012). Engelman and colleagues established a gefitinib-resistant HCC827GR cell line generated by the long-term treatment of HCC827 cells with gefitinib and found gefitinib resistance by the amplification of MET via the activation of ERBB3 signaling (Engelman et al., 2007). Therefore, the development of a dual inhibitor of EGFR and MET that can overcome the resistance mechanism of gefitinib has the potential to successfully treat NSCLC.

The purpose of present study was to determine the underlying molecular mechanism of cell growth inhibition by PPT treatment in gefitinib-resistant NSCLC cells. We investigated cell cycle regulation and apoptosis induction through the dual inhibition of EGFR and MET in HCC827GR cells, a previously established gefitinib-resistant cell line. To investigate the hypothesis, we examined EGFR and MET activation, the expression of downstream molecules, and apoptosis induction through the kinase assay, pull-down assay, computational docking model, western blotting, and various flow cytometry analyses. Apoptosis induction by PPT treatment was verified by treatment with N-acetyl cysteine, a reactive oxygen species (ROS) scavenger, and Z-VAD-FMK, a caspase inhibitor. The anticancer activity of PPT can provide insight into the therapeutic aspect of gefitinib-resistant NSCLC, indicating that PPT may be a candidate for cancer prevention and treatment.

MATERIALS AND METHODS

Reagents and antibodies

The PPT (>95%) was purchased from Sigma-Aldrich (St. Louis, MO, USA). Roswell Park Memorial Institute (RPMI)-1640 Medium, phosphate buffered saline (PBS), fetal bovine serum (FBS), penicillin and streptomycin and trypsin were purchased from Hyclone (Logan, UT, USA). 3-(4,5-dimethylthiazol-2-yl)-2,5-diphenyltetrazolium bromide (MTT), Basal Medium Eagle, and dimethyl-sulfoxide (DMSO) were purchased from Sigma-Aldrich (St. Louis, MO, USA). The primary antibodies against cyclin B1, cdc2, p21, actin, GRP78, CCAAT/enhancer-binding protein homologous protein (CHOP), death receptor (DR)5, DR4, Bcl-xl, Mcl-1, Bad, Apoptotic protease activating factor-1 (Apaf-1), Poly (ADP-Ribose) Polymerase (PARP), cytochrome C (cyto C), α-tubulin, and COX4 were obtained from Santa Cruz Biotechnology (Santa Cruz, CA, USA). Antibodies against p-EGFR (Tyr1068), EGFR, p-MET (Tyr1234/1235), MET, p-AKT (Ser473), AKT, p-ERK (Thr202/Tyr204), and ERK were purchased from Cell Signaling Biotechnology (Beverly, MA, USA).

Cell culture

HCC827GR (MET-amplified and gefitinib-resistant HCC827) cells were kindly obtained by professor Pasi A. Jänne, Department of Medical Oncology, Dana-Farber Cancer Institute, Boston, MA, USA. The cells were cultured in RPMI-1640 medium with 10% FBS and 100 U/mL penicillin-streptomycin and incubated at 37°C in a 95% humidified and 5% CO$_2$ atmosphere.

MTT assay

Cells were plated into 96-well plates at a density of 5.5×10^3 cells/well and allowed to incubate for 24 h. The cells were treated with DMSO or PPT for 24 h or 48 h. After incubation, cells were reacted with MTT reagents for 1 h at 37°C. Then, supernatant containing culture medium and MTT reagents was removed from the each well and formazan crystals were dissolved with 100 μL of DMSO. The absorbance at 570 nm was measured using a Multiscan GO spectrophotometer (Thermo Scientific, Vantaa, Finland).

Anchorage-independent cell growth assay

Top agar (3%) and culture medium containing BME, 10% FBS, 2 mM L-glutamine and 5 μg/mL gentamicin was mixed with the cell suspension and then added into 6-well plate (8,000 cells/well), which were previously based with 0.6% agar in the same medium. Various concentrations of DMSO or PPT were added to bottom and upper layer. The plates were incubated at 37°C for 2 weeks and the colonies were captured and counted by light microscope (Leica Microsystems, Wetzlar, Germany).

Annexin V/7-AAD staining assay

HCC827GR (5.5×10^4) cells per well in 6-well plate were seeded and treated with DMSO or PPT for 48 h. Cells were collected and processed as described in the Muse™ Annexin V & Dead Cell Kit manual (MCH100105, Merck Millipore, Billerica, MA, USA). Annexin V/7-aminoactinomycin D (7-AAD) stained apoptotic cells were measured using Muse™ Cell Analyzer (Merck Millipore).

Cell cycle analysis

For cell cycle distribution analysis, HCC827GR were seeded with density of 5.5×10⁴ cells per well in 6-well culture plates. After incubation overnight, the cells were treated with DMSO or PPT for 48 h, and harvested using trypsin. Cells were rinsed with cold 1X PBS and fixed in cold 70% ethanol overnight at −20°C. Then cells were washed with 1X PBS and resuspended with Muse™ Cell Cycle Reagent MCH100106 (Merck Millipore) and incubated at room temperature (RT) for 30 min in the dark. The quantitation of cell cycle distribution was measured by a Muse™ Cell Analyzer.

Western blotting

Cells lysate was collected following lysis in RIPA buffer (iN-tRON Biotechnology, Seongnam, Korea) for 10 min at 4°C and sonicated then centrifuged at 13,000 rpm for 30 min. Protein concentrations were determined by using the Bio-Rad DC Protein Assay kit (Bio-Rad, Hercules, CA, USA). Target proteins were separated by SDS-polyacrylamide gel electrophoresis and transferred to polyvinylidene fluoride membranes. Membranes were incubated with 3% or 5% skim milk in 1X PBST (PBS with 0.1% Tween 20) for 2 h, and probed with specific primary antibodies. Washed membranes with 1X PBST were incubated with the appropriate horseradish peroxidase-conjugated secondary antibodies at RT for 2 h. The specific protein bands were detected by the Image Quant LAS 500 (GE Healthcare, Uppsala, Sweden).

Pull-down assay

To analyze the interaction between PPT and EGFR or MET, the HCC827GR cell lysate was immobilized to Sepharose 4B beads or PPT-Sepharose 4B beads. A total protein extract was incubated for 12 h at 4°C with PPT-Sepharose 4B beads, or negative control-Sepharose 4B beads in reaction buffer containing 50 mM Tris (pH 7.5), 5 mM EDTA, 150 mM NaCl, 1 mM/L dithiothreitol, 0.01% Nonidet P-40, 2 μg/mL bovine serum albumin, 0.02 mM phenylmethylsulfonyl fluoride and 1X proteinase inhibitor. The beads were washed six times with washing buffer containing 50 mM Tris (pH 7.5), 5 mM EDTA, 150 mM NaCl, 1 mM dithiothreitol, 0.01% Nonidet P-40 and 0.02 mM phenylmethylsulfonyl fluoride, and then eluted with SDS sample buffer. Eluted proteins were identified using SDS- polyacrylamide gel electrophoresis and western blotting analysis.

Kinase assay

EGFR and MET kinase activity was measured by using the EGFR (#3831) and MET (#3361) kinase enzyme system (Promega, Madison, WI, USA) and ADP-Glo kinase assay kit (Promega) according to the manufacturer's instructions. The 1.8 ng/μL EGFR and 7 ng/μL MET were incubated in a 384-well white plate with 0.1, 0.2, 0.3, and 0.4 μM of PPT or 1 μM of gefitinib or 2 nM of savolitinib, 5 μM or 10 μM of ATP, 0.2 μg/μL of substrates and kinase reaction buffer containing 40 mM Tris (pH 7.5), 20 mM MgCl₂, 0.1 mg/mL BSA, 50 μM DTT, 2 mM MnCl₂ and 100 μM sodium vanadate at RT for 1 h. To complete the kinase reaction and depletes the remaining ATP, ADP-Glo reagent was added to each well and allowed to react at RT for 40 min. Then kinase activity detection reagent was added to each well and incubated at RT for 30 min. Kinase activity was determined by Centro LB 960 microplate luminometer (Berthold Technologies, Wildbad, Germany) for 0.5 s.

Molecular modelling

To predict the binding mode of the receptor tyrosine kinases, we performed a molecular docking simulation using Autodock Vina (Trott and Olson, 2010). PDB files 4XYF and 1M17 were downloaded from protein data bank for the structures of c-Met and EGFR. The PDB file for picropodophyllotoxin was generated with Pymol using the structure data file. To ensure the unbiased search, the search grid was set to cover the entire surface of the protein. Ten modes were reported after running with Autodock Vina for each docking modelling, and the best mode was chosen for structure depiction.

Reactive oxygen species (ROS) measurements

Using the Muse™ Oxidative Stress Kit (MCH100111, Merck Millipore), ROS generation was determined. Briefly, cells were exposed to 0.2, 0.3, and 0.4 μM of PPT for 48 h and washed with 1X assay buffer then incubated in Muse™ Oxidative Stress Reagent working solution at 37°C for 30 min. The samples were analyzed by using Muse™ Cell Analyzer.

Mitochondrial membrane potential (MMP) assay

Changes of the MMP in HCC827GR cells were examined using a Muse™ MitoPotential Kit (MCH100110, Merck Millipore), according to the manufacturer's instructed protocol. Cells were collected and rinsed with 1X assay buffer. Then cells were resuspended in Muse™ MitoPotential working solution and incubated at 37°C for 20 min. After incubation with 7-AAD at RT for 5 min, MMP was measured using Muse™ Cell Analyzer.

Isolation of cytosol and mitochondrial fractionation

PPT-treated or –untreated HCC827GR cells were resuspended in plasma membrane extraction buffer [250 mM sucrose, 10 mM HEPES (pH 8.0), 10 mM KCl, 1.5 mM MgCl₂·6H₂O, 1 mM EDTA, 1 mM EGTA, 0.1 mM phenylmethylsulfonyl fluoride, 0.01 mg/mL aprotinin, 0.01 mg/mL leupeptin] before homogenization using a 0.1% of digitonin for 5 min. The homogenized cells were centrifuged at 13,000 rpm for 5 min. The supernatant was furtherly centrifuged at 13,000 rpm for 30 min (the cytosolic fraction). The remaining pellet was washed with plasma membrane extraction buffer and centrifuged at 13,000 rpm for 5 min. The pellet was resuspended in plasma membrane extraction buffer and 0.5% of triton X-100, and centrifuged at 13,000 rpm for 30 min (the mitochondrial fraction). The cyto C level of each fraction was visualized by western blotting.

Multi-caspase assay

Multi-caspase (caspase-1, -3, -4, -5, -6, -7, -8, and -9) activity was analyzed by Muse™ Multi-Caspase Kit (MCH100109, Merck Millipore). HCC827GR (5.5×10⁴ cells/well) cells were plated in 6-well plate and allowed to attach for 24 h. After treatment of DMSO or PPT for 48 h, cells were washed with 1X caspase buffer and incubated with Muse™ Multi-Caspase Reagent working solution at 37°C for 30 min. Cells were analyzed with Muse™ Cell Analyzer following add Muse™ Caspase 7-AAD working solution for 5 min.

Statistical analysis

Statistical tests were performed using one-way ANOVA done on Prism 5.0 statistical package (GraphPad Software, San Diego, CA, USA) and all data were expressed as mean
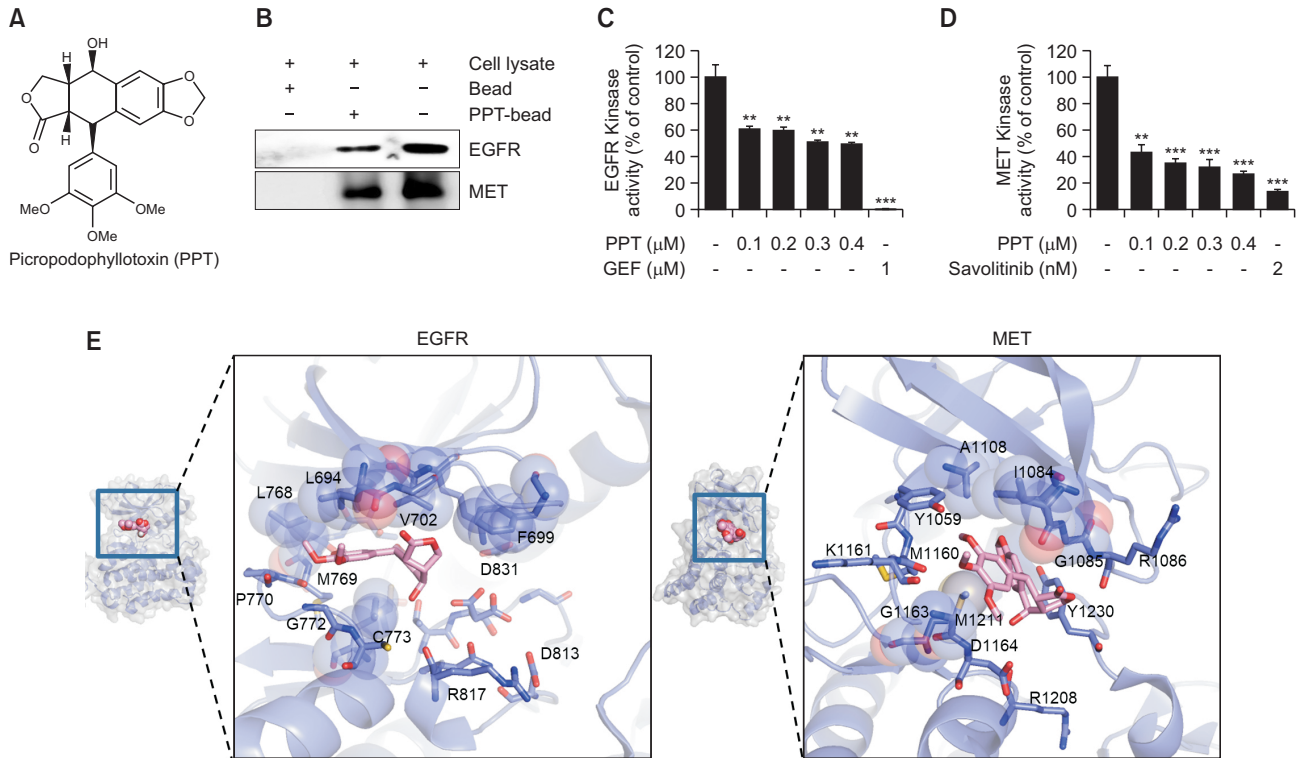
Fig. 1. Effects of PPT on EGFR or MET binding and kinase activities. (A) PPT chemical structure. (B) EGFR or MET protein interaction with PPT. Pull-down assay was performed with HCC827GR cell lysate using Sepharose 4B beads or PPT-Sepharose 4B beads: lane 1, Sepharose 4B beads, lane 2, PPT-Sepharose 4B beads, Lane 3, input control. (C, D) *In vitro* ADP-Glo kinase assay was using EGFR (C) or MET (D) kinase enzyme system. The values indicate mean ± SD from three independent experiments. **$p<0.01$ or ***$p<0.001$ compared with the control. (E) The predicted binding sites of PPT in EGFR and MET. The ATP binding pockets of receptor tyrosine kinases shown with surface representation were tightly occupied by PPT (spheres). The ATP pocket was zoomed in. PPT (pink) and the amino acids (purple) within 4 Angstroms are depicted in stick representation. Amino acids possibly involved with hydrophobic interactions are shown with balls.

± standard deviation (SD). A difference of *p* values<0.05 was considered as significant.

RESULTS

PPT directly binds with either EGFR or MET and inhibits both EGFR and MET kinase activity

To identify EGFR and MET targeting by PPT treatment, we performed an *ex vivo* pull-down assay and determined EGFR and MET kinase activity (Fig. 1B-1D). The results showed that PPT was bound to either EGFR or MET in HCC827GR cell lysates (Fig. 1B). In the kinase assay results, the positive controls gefitinib and savolitinib were used as EGFR and MET clinical drugs, respectively. PPT treatment (0.1, 0.2, 0.3, and 0.4 μM) significantly inhibited EGFR (39.3, 40.1, 48.6, and 50.2%) and MET (56.7, 64.8, 68.0, and 73.0%) kinase activity, respectively, compared to the untreated control group (Fig. 1C, 1D). The molecular modeling obtained from Autodock Vina simulations located PPT in the ATP-binding sites of both receptor tyrosine kinases (Fig. 1E). For interactions with EGFR, the backbone amino groups of Gly772 and Met769 and the hydroxyl groups of Thr766 and Thr830 were in positions to form hydrogen bonds with PPT (Fig. 1E left). For interactions with MET, the backbone amino group from Arg1086 and the side chain hydroxyl group from Tyr1230 were likely to form

hydrogen bonds with PPT (Fig. 1E right). In addition, hydrophobic residues, such as Leu694 and Leu768 in EGFR and Ile1084 and Ala1108 in MET, were in close contact with PPT. These results suggested that PPT inhibited EGFR and MET kinase activity by binding in the ATP-binding pocket of EGFR and MET, respectively.

PPT inhibits cell viability in gefitinib-resistant HCC827GR cells

We used HCC827GR cells to observe the effects of PPT in a gefitinib-resistant NSCLC cell line expressing both EGFR and MET. To examine the effect of PPT on the viability of HCC827GR cells, we performed an MTT assay. The results showed that 0.1, 0.2, 0.3, and 0.4 μM PPT decreased cell viability significantly to 94.3, 86.6, 70.6, and 44.4% at 24 h and to 94.1, 82.9, 68.0, and 34.3% at 48 h, respectively (Fig. 2A). Treatment with either gefitinib or savolitinib decreased HCC827GR cell viability, and cotreatment with gefitinib and savolitinib decreased viability to 74.9 and 39.6% at 24 h and 48 h, respectively (Fig. 2A). The inhibitory effects of PPT on cell viability were confirmed by anchorage-independent colony growth (Fig. 2B-2D). PPT inhibited colony growth to 42.9, 63.2, 71.4, and 94.7% in a dose-dependent manner (0.1, 0.2, 0.3, and 0.4 μM, respectively) (Fig. 2B, 2C). Also, cotreatment with gefitinib and savolitinib suppressed viability to 84.2%, even though single treatments did not affect cell viability (Fig.
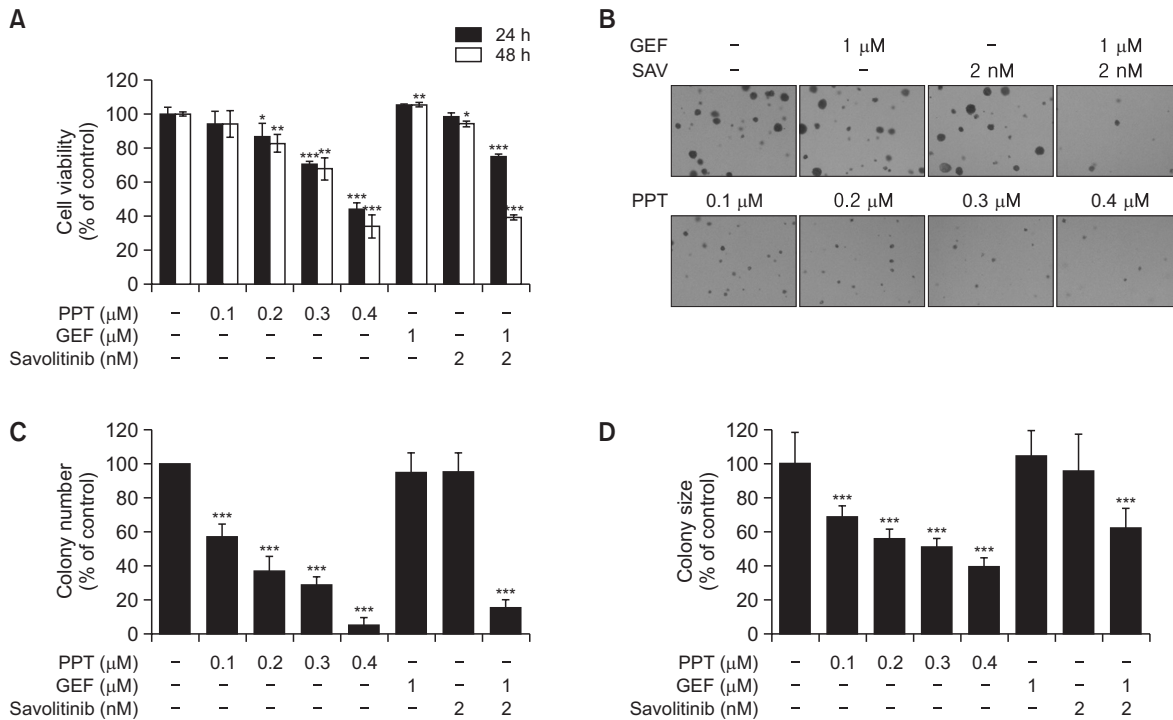
Fig. 2. Effects of PPT on cell viability and colony formation. (A) MTT assay determined cell viability in HCC827GR (gefitinib-resistant) following treatment PPT, GEF, or Savolitinib. Values shown in the graph are mean ± SD. *$p<0.05$, **$p<0.01$, or ***$p<0.001$ compared with the control. (B-D) Soft agar assay determined colony forming ability in HCC827GR cells treated with PPT, GEF, or SAV. After 14 days of culture, the colonies picture was captured (B) and colonies number (C) and over 50 μm diameter size (D) were counted under microscope. Results are representative of triplicate experiments. ***$p<0.001$ compared with the control.

2B, 2C). In addition, the effect of PPT on colony size showed similar inhibitions (Fig. 2D). These results indicated that PPT decreased cell viability and colony growth in gefitinib-resistant HCC827GR cells.

PPT induced apoptosis and G2/M phase cell cycle arrest in HCC827GR cells

We measured the effect of PPT on apoptosis and the cell cycle in HCC827GR cells by flow cytometry analysis (Fig. 3). To evaluate apoptosis, HCC827GR cells treated with PPT (0.2, 0.3, and 0.4 μM) were stained with annexin V and 7-AAD (Fig. 3A). The percent of total apoptosis which are right down (early, annexin V+/7-AAD-) plus right upper (late, annexin V+/7-AAD+) population, were increased to 20.6, 26.5, and 36.3% at 0.2, 0.3, and 0.4 μM of PPT, respectively (Fig. 3A). In the cell cycle analysis, the treatment of HCC827GR cells with 0.2, 0.3, and 0.4 μM PPT significantly increased the subG1 population to 10.1, 25.7, and 58.8%, respectively, compared to the untreated group (2.5%) (Fig. 3B). In addition, the proportion of G2/M phase HCC827GR cells following PPT treatment increased to 35.3, 35.5, and 48.6% compared to untreated cells (30.0%), whereas cells in the G0/G1 phase were decreased in a concentration-dependent manner and those in the S phase didn't much changed (Fig. 3C). These results were confirmed by detecting the expression of G2/M phase regulatory markers including cyclin B1, cdc2, and p21 using Western blotting (Fig. 3D). As shown in Fig. 3D, PPT reduced the expression of cyclin B1 and cdc2 in HCC827GR cells in a dose-dependent manner and increased p21 levels compared

to controls. Therefore, the results demonstrated that the anti-proliferative effects of PPT in HCC827GR cells induced apoptosis and G2/M cell cycle arrest.

PPT down-regulates EGFR and MET-mediated signaling pathways

Because PPT bound to both EGFR and MET and inhibited kinase activity, we performed western blotting to identify whether PPT regulated EGFR and MET-mediated downstream signaling proteins including AKT and ERK (Fig. 4). Treatment of HCC827GR cells with increasing concentrations of PPT suppressed the phosphorylation of EGFR and MET compared to controls, whereas the total form of each was unchanged. The phosphorylation of the downstream effectors, AKT and ERK was also decreased by PPT treatment. These results suggested that the direct targeting of EGFR and MET by PPT decreased EGFR- and MET-related signaling pathways.

PPT increases ROS generation and ER stress in HCC827GR cells

Endoplasmic reticulum (ER) stress and redox stress were reported to be highly correlated with cell homeostasis and apoptosis, and cellular stress could stimulate apoptosis signaling pathways (Cao and Kaufman, 2014). Thus, since PPT induced apoptosis in HCC827GR cells, we examined the effects of PPT on ROS and ER stress levels by flow cytometry analysis and western blotting assays (Fig. 5). PPT treatment at 0.2, 0.3, and 0.4 μM for 48 h increased ROS production to
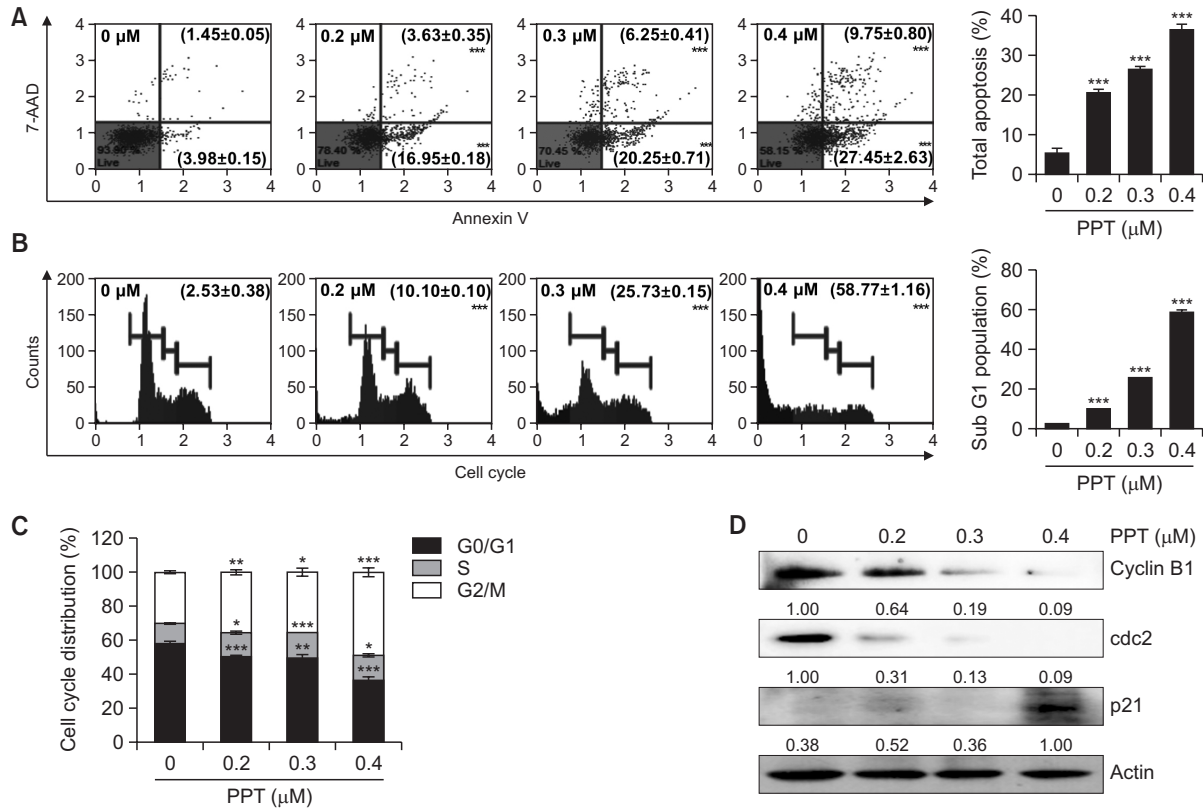
Fig. 3. Effects of PPT on cell apoptosis and cell cycle. (A) Flow cytometry analysis of apoptosis with Annexin V/7-aminoactinomycin D (7-AAD) binding to HCC827GR cells after treatment with PPT for 48 h. The lower left represents living cells (Annexin V−/7-AAD−), the lower right represents early apoptotic cells (Annexin V+/7-AAD−), the upper right represents late apoptotic cells (Annexin V+/7-AAD+), and the upper left represents dead cells (Annexin V−/7-AAD+) (left). Numbers in each quadrant are percentages of early and late apoptotic cells. Data are mean ± SD. Total apoptosis percent were showed with histogram graph (right). (B) PPT-untreated or –treated NSCLC cells were analyzed by Muse™ Cell Analyzer for cell cycle analysis (left). The subG1 population percent were showed with histogram graph (right). (C) G0/G1, S and G2/M phase population of cell cycle were presented by percent. Each value represents the mean ± SD (n=3). *$p<0.05$, **$p<0.01$, or ***$p<0.001$ compared with the control. (D) The expression of G2/M phase cell cycle-related proteins was confirmed by western blotting in HCC827 cells. Actin was used as a loading control.

33.7, 56.8, and 66.4%, respectively, compared to untreated cells (28.5%) (Fig. 5A). To verify ROS induction, we treated HCC827GR cells with NAC, a ROS scavenger, and measured cell viability (Fig. 5B). The results showed that treatment with 0.4 μM PPT decreased cell viability to 40.7%, whereas treatment with PPT plus NAC decreased cell viability to 74.0% (Fig. 5B). In addition, PPT treatment of HCC827GR cells induced the expression of ER stress markers including GRP78 and CHOP in a dose-dependent manner (Fig. 5C). CHOP is a transcription factor for the expression of pro-apoptotic genes such as DR in cancer cells (Cao and Kaufman, 2014). As shown in Fig. 5C, DR5 and DR4 expression was elevated in HCC827GR cells after treatment with PPT for 48 h. These results indicated that the apoptosis of HCC827GR cells by PPT treatment was associated with ROS and ER stress induction.

PPT up-regulates mitochondrial membrane potential dysfunction and caspase activity in HCC827GR cells

To investigate HCC827GR cell apoptosis induced by PPT treatment via the mitochondrial-mediated pathway, we measured changes in mitochondrial membrane potential (MMP), apoptosis-related protein expression, and multi-caspase activity (Fig. 6, 7). The total percentage of depolarized cells after

PPT treatment (0.2, 0.3, and 0.4 μM) for 48 h increased to 8.9, 18.2, and 33.6%, respectively, in the MMP assay compared to controls (5.9%) (Fig. 6A). As shown in the western blot results, the expression of anti-apoptotic marker proteins Mcl-1 and Bcl-xl was reduced by PPT. However, the level of the pro-apoptotic protein Bad was induced in HCC827GR cells treated with PPT in a dose-dependent manner (Fig. 6B). Moreover, the expression of cytosolic cyto C was increased, whereas mitochondrial cyto C was decreased. Apaf-1 expression was increased and total PARP levels were decreased in a dose-dependent manner (Fig. 6B). Next, we determined whether PPT induced apoptosis in HCC827GR cells through a caspase-dependent pathway by measuring caspase-1, -3, -4, -5, -6, -7, -8, and -9 using the Muse™ Cell Analyzer. The results revealed that multi-caspase activity including caspase-1, -3, -4, -5, -6, -7, -8, and -9 was increased to 11.1, 19.4, and 32.2% in HCC827GR cells treated with PPT (0.2, 0.3, and 0.4 μM, respectively) for 48 h (Fig. 7A, 7B). To evaluate caspase-dependent apoptosis by PPT treatment, we used the pan-caspase inhibitor Z-VAD-FMK to pretreat HCC827 cells for 3 h and later exposed them to PPT for 48 h. The MTT assay results showed that cell viability was reduced by 68.7% by treatment with PPT alone, whereas it was only reduced by 17.8% by treatment with Z-
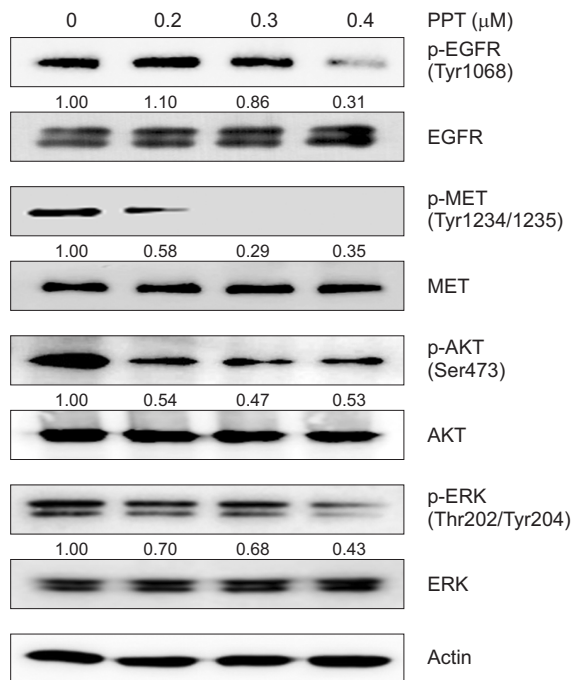
Fig. 4. Effects of PPT on EGFR or MET mediated signaling pathways. Cells were treated with PPT at the indicated concentration for 48 h, then protein expression levels were determined. HCC-827GR cell lysates were subjected to western blotting to detect of p-EGFR (Tyr1068), EGFR, p-MET (Tyr1234/1235), MET, p-AKT (Ser473), AKT, p-ERK (Thr202/Tyr204) and ERK antibodies.

VAD-FMK plus PPT (Fig. 7C). These results showed that PPT induced apoptosis in HCC827GR cells via a mitochondria (intrinsic)- and caspase-dependent pathway.

DISCUSSION

EGFR-targeted therapy for lung cancer patients showed a new paradigm in 2000 when first-generation tyrosine kinase inhibitors (TKI) including gefitinib, erlotinib, and icotinib were introduced. These EGFR-TKIs reversibly bind to the ATP-binding pocket of EGFR, generating high responses in lung cancer patients harboring EGFR-activating mutants (~70%) (Jackman *et al.*, 2010).

Drug resistances after treatment with gefitinib for a while are appeared by EGFR-second mutation and EGFR-independent alteration. The T790M EGFR mutation is found in ~50% of EGFR-mediated NSCLC patients, and the mutation from threonine to methionine leads to ATP-binding compared to gefitinib (Kobayashi *et al.*, 2005; Johnson *et al.*, 2022). In contrast, MET amplification is shown in 5-20% of EGFR-TKI acquired resistance (Kosaka *et al.*, 2011; Brugger and Thomas, 2012; Johnson *et al.*, 2022) and it is mediated by ErbB2 amplification (Schulze *et al.*, 2005). Because the downstream cascades of EGFR and MET signaling pathways including AKT and ERK are overlapped, inhibiting both EGFR and MET is a potential strategy compared to treatment with single drug (Guo *et al.*, 2008; Puri and Salgia, 2008). PPT bound EGFR and MET proteins at predicted sites of Gly772 and Met769 in EGFR, and Arg1086 and Tyr1230 in MET, thus inhibiting their activity (Fig. 1B-1E). Then, we confirmed that inhibiting both
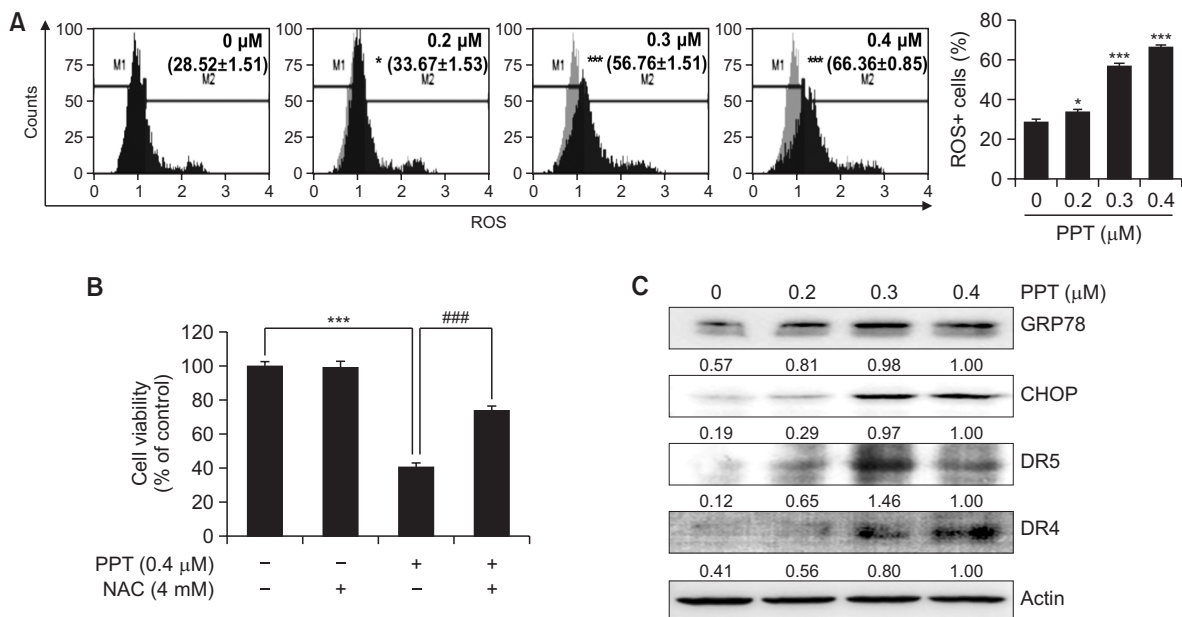
Fig. 5. Effect of PPT on ROS and ER-stress. (A) HCC827GR cells were exposed to PPT (0.2, 0.3, and 0.4 μM) for 48 h and intracellular ROS fluorescence was immediately detected by Muse™ Cell Analyzer. Gray peaks are control cells without PPT treatment, and black peaks are PPT-treated cells. ROS-positive values are means ± SD (left). The percent of ROS positive cells were showed with histogram graph (right). *$p<0.05$ or ***$p<0.001$ compared with the control. (B) Cells were treated with, NAC only or cotreated with PPT and NAC and measured the cell viability. Values shown in the histogram represent mean ± SD. ***$p<0.001$ compared with the control. ###$p<0.001$ significantly different from PPT-treated cells. (C) After treatment of PPT, the protein expression was assessed by western blotting using specific antibodies such as GRP78, CHOP, DR5, and DR4. Actin was used as a loading control.
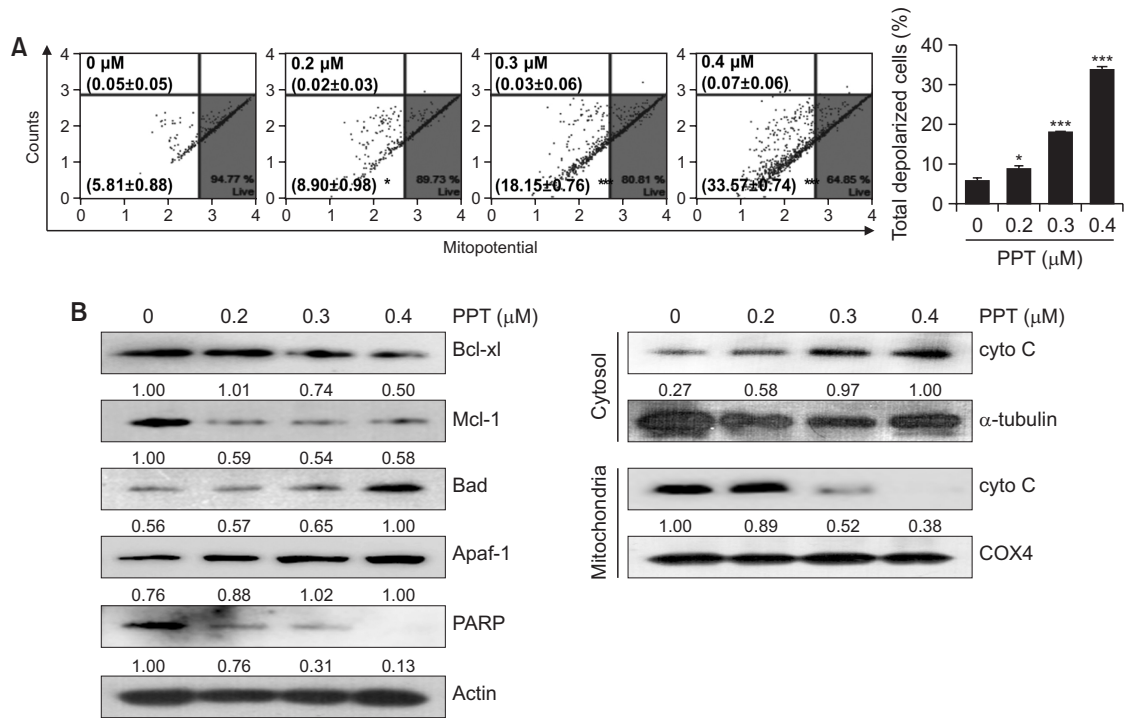
Fig. 6. Effect of PPT on mitochondrial membrane potential (MMP). HCC827GR cells were treated with 0, 0.2, 0.3, and 0.4 μM of PPT for 48 h. (A) MMP changes were determined by Muse™ Cell Analyzer. The scatter plots on the left quadrant indicates depolarization of the MMP (left). Values are means ± SD. The percent of total depolarized cells were showed with histogram graph (right). Results are representative of three independent experiments. *$p<0.05$ or ***$p<0.001$ compared with the control. (B) Cell lysates were performed by western blotting with antibodies against the Bcl-xl, Mcl-1, Bad, Apaf-1, PARP, and cyto c (cytosolic and mitochondrial). α-Tubulin and COX4 were used as loading controls for cyto c in cytosol and mitochondria, and actin was used as the internal control for equivalent loading.
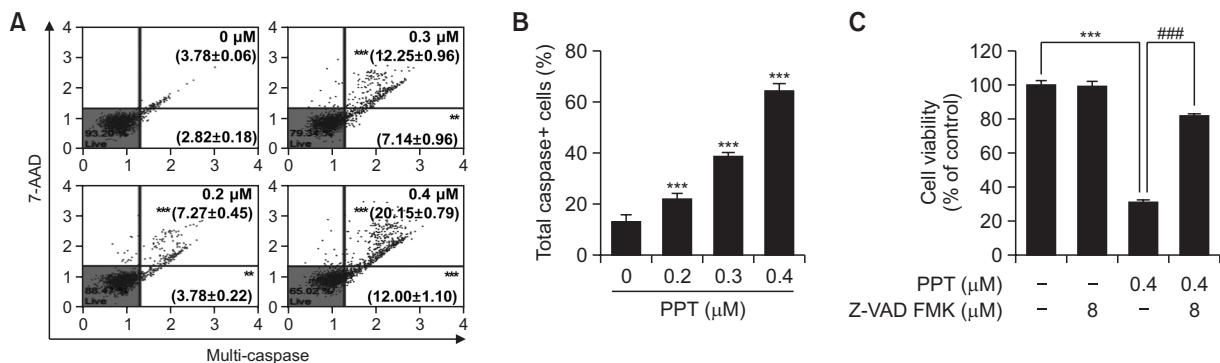
Fig. 7. Effect of PPT on caspase activities. (A) Cells were treated with 0.2, 0.3, and 0.4 μM of PPT for 48 h, and multi-casapse (-1, -3, -4, -5, -6, -7, -8, and -9) activity was measured by Muse™ Cell Analyzer. Data are presented as mean ± SD of three independent experiments. (B) The percent of total caspase positive cells were showed with histogram graph. ***$p<0.001$ compared with the control. (C) Cells were pretreated with or without 8 μM of Z-VAD-FMK for 3 h and then exposed or not to the 0.4 μM of PPT for 48 h. After treatment, MTT assay was performed and the values were expressed as means ± SD. ***$p<0.001$, significantly different from PPT-untreated control cells. ###$p<0.001$, significantly different from PPT-treated cells.

EGFR and MET was effective in inhibiting cell growth. In fact, a single treatment with gefitinib, an EGFR inhibitor, or savolitinib, a MET inhibitor, failed to significantly inhibit cell viability and colony formation (Fig. 2), whereas treatment with both gefitinib and savolitinib significantly suppressed cell growth, colony numbers, and size. PPT dose-dependently inhibited cell viability and colony growth, as well as induced apoptosis and cell cycle arrest (Fig. 2, 3). The results indicate that PPT effectively inhibited gefitinib-resistant NSCLC by simultaneously obstructing EGFR and MET. Furthermore, the activation of AKT and ERK involved in the downstream signaling pathways of EGFR and MET for enhancing cancer cell survival and proliferation, were dose-dependently suppressed following decreases in p-EGFR and -MET expression (Fig. 4).

Apoptosis is induced mainly by extrinsic and intrinsic pathways via DNA damage and cellular stress (Cao and Kaufman, 2014; Perillo *et al*., 2020). Excessive ROS levels induce cancer cell death by intrinsic apoptotic pathways. This was verified by the PPT treatment of gefitinib-resistant HCC827GR cells. In these cells, PPT treatment-induced ROS production was prevented by treatment with NAC, a ROS scavenger (Fig. 5A, 5B). ER stress-related markers GRP78 and CHOP and their downstream DR5 and DR4 levels were elevated by PPT treatment (Fig. 5C). Increases in ROS levels induce MMP dysfunction and regulate related known signaling makers (Zorov *et al*., 2014; Perillo *et al*., 2020). PPT decreased Bcl-xl, Mcl, mitochondrial cyto C, and PARP levels, and increased Bad, cytosolic cyto C, and Apaf-1 expression (Fig. 6). Caspase activity was increased in the late step of apoptosis (Li *et al*., 1997; Kim *et al*., 2021). PPT induced multi-caspase activity, which was verified by measuring cell viability after treatment with the caspase inhibitor Z-VAD-FMK (Fig. 7).

In conclusion, PPT directly targeted both EGFR and MET to inhibit cell proliferation and induce apoptosis in gefitinib-resistant NSCLC cells. Therefore, PPT can be considered a therapeutic agent for the treatment of gefitinib-resistant non-small cell lung cancer.

CONFLICT OF INTEREST

The authors have no conflicts of interest relevant to this study to disclose.

ACKNOWLEDGMENTS

REFERENCES

Akhtar, N. and Bansal, J. G. (2017) Risk factors of lung cancer in non-smoker. *Curr. Probl. Cancer* **41**, 328-339.

Brugger, W. and Thomas, M. (2012) EGFR-TKI resistant non-small cell lung cancer (NSCLC): new developments and implications for future treatment. *Lung Cancer* **77**, 2-8.

Canel, C., Moraes, R. M., Dayan, F. E. and Ferreira, D. (2000) Podophyllotoxin. *Phytochemistry* **54**, 115-120.

Cao, S. S. and Kaufman, R. J. (2014) Endoplasmic reticulum stress and oxidative stress in cell fate decision and human disease. *Antioxid. Redox Signal.* **21**, 396-413.

Engelman, J. A. and Janne, P. A. (2008) Mechanisms of acquired resistance to epidermal growth factor receptor tyrosine kinase inhibitors in non-small cell lung cancer. *Clin. Cancer Res.* **14**, 2895-2899.

Engelman, J. A., Zejnullahu, K., Mitsudomi, T., Song, Y., Hyland, C., Park, J. O., Lindeman, N., Gale, C. M., Zhao, X., Christensen, J., Kosaka, T., Holmes, A. J., Rogers, A. M., Cappuzzo, F., Mok, T., Lee, C., Johnson, B. E., Cantley, L. C. and Janne, P. A. (2007) MET amplification leads to gefitinib resistance in lung cancer by activating ERBB3 signaling. *Science* **316**, 1039-1043.

Girnita, A., Girnita, L., del Prete, F., Bartolazzi, A., Larsson, O. and Axelson, M. (2004) Cyclolignans as inhibitors of the insulin-like growth factor-1 receptor and malignant cell growth. *Cancer Res.* **64**, 236-242.

Gordaliza, M., Garcia, P. A., del Corral, J. M., Castro, M. A. and Go-mez-Zurita, M. A. (2004) Podophyllotoxin: distribution, sources, applications and new cytotoxic derivatives. *Toxicon* **44**, 441-459.

Griffin, R. and Ramirez, R. A. (2017) Molecular targets in non-small cell lung cancer. *Ochsner J.* **17**, 388-392.

Guo, A., Villen, J., Kornhauser, J., Lee, K. A., Stokes, M. P., Rikova, K., Possemato, A., Nardone, J., Innocenti, G., Wetzel, R., Wang, Y., MacNeill, J., Mitchell, J., Gygi, S. P., Rush, J., Polakiewicz, R. D. and Comb, M. J. (2008) Signaling networks assembled by oncogenic EGFR and c-Met. *Proc. Natl. Acad. Sci. U. S. A.* **105**, 692-697.

International Agency for Research on Cancer (2020) GLOBOCAN Lung Cancer Facts Sheet 2020. World Health Organization. Available from: https://gco.iarc.fr/today/data/factsheets/cancers/15-Lung-fact-sheet.pdf/.

Jackman, D., Pao, W., Riely, G. J., Engelman, J. A., Kris, M. G., Janne, P. A., Lynch, T., Johnson, B. E. and Miller, V. A. (2010) Clinical definition of acquired resistance to epidermal growth factor receptor tyrosine kinase inhibitors in non-small-cell lung cancer. *J. Clin. Oncol.* **28**, 357-360.

Johnson, M., Garassino, M. C., Mok, T. and Mitsudomi, T. (2022) Treatment strategies and outcomes for patients with EGFR-mutant non-small cell lung cancer resistant to EGFR tyrosine kinase inhibitors: focus on novel therapies. *Lung Cancer* **170**, 41-51.

Kim, H. S., Oh, H. N., Kwak, A. W., Kim, E., Lee, M. H., Seo, J. H., Cho, S. S., Yoon, G., Chae, J. I. and Shim, J. H. (2021) Deoxypodophyllotoxin inhibits cell growth and induces apoptosis by blocking EGFR and MET in gefitinib-resistant non-small cell lung cancer. *J. Microbiol. Biotechnol.* **31**, 559-569.

Kobayashi, S., Boggon, T. J., Dayaram, T., Janne, P. A., Kocher, O., Meyerson, M., Johnson, B. E., Eck, M. J., Tenen, D. G. and Halmos, B. (2005) EGFR mutation and resistance of non-small-cell lung cancer to gefitinib. *N. Engl. J. Med.* **352**, 786-792.

Kosaka, T., Yamaki, E., Mogi, A. and Kuwano, H. (2011) Mechanisms of resistance to EGFR TKIs and development of a new generation of drugs in non-small-cell lung cancer. *J. Biomed. Biotechnol.* **2011**, 165214.

Kris, M. G., Natale, R. B., Herbst, R. S., Lynch, T. J., Jr., Prager, D., Belani, C. P., Schiller, J. H., Kelly, K., Spiridonidis, H., Sandler, A., Albain, K. S., Cella, D., Wolf, M. K., Averbuch, S. D., Ochs, J. J. and Kay, A. C. (2003) Efficacy of gefitinib, an inhibitor of the epidermal growth factor receptor tyrosine kinase, in symptomatic patients with non-small cell lung cancer: a randomized trial. *JAMA* **290**, 2149-2158.

Kwak, A. W., Yoon, G., Lee, M. H., Cho, S. S., Shim, J. H. and Chae, J. I. (2020) Picropodophyllotoxin, an epimer of podophyllotoxin, causes apoptosis of human esophageal squamous cell carcinoma cells through ROS-mediated JNK/P38 MAPK pathways. *Int. J. Mol. Sci.* **21**, 4640.

Lee, S. O., Kwak, A. W., Lee, M. H., Seo, J. H., Cho, S. S., Yoon, G., Chae, J. I., Joo, S. H. and Shim, J. H. (2021) Picropodophyllotoxin induces G1 cell cycle arrest and apoptosis in human colorectal cancer cells via ROS generation and activation of p38 MAPK signaling pathway. *J. Microbiol. Biotechnol.* **31**, 1615-1623.

Li, P., Nijhawan, D., Budihardjo, I., Srinivasula, S. M., Ahmad, M., Alnemri, E. S. and Wang, X. (1997) Cytochrome c and dATP-dependent formation of Apaf-1/caspase-9 complex initiates an apoptotic protease cascade. *Cell* **91**, 479-489.

Miller, K. D., Nogueira, L., Devasia, T., Mariotto, A. B., Yabroff, K. R., Jemal, A., Kramer, J. and Siegel, R. L. (2022) Cancer treatment and survivorship statistics, 2022. *CA Cancer J. Clin.* **72**, 409-436.

Perillo, B., Di Donato, M., Pezone, A., Di Zazzo, E., Giovannelli, P., Galasso, G., Castoria, G. and Migliaccio, A. (2020) ROS in cancer therapy: the bright side of the moon. *Exp. Mol. Med.* **52**, 192-203.

Puri, N. and Salgia, R. (2008) Synergism of EGFR and c-Met pathways, cross-talk and inhibition, in non-small cell lung cancer. *J. Carcinog.* **7**, 9.

Schulze, W. X., Deng, L. and Mann, M. (2005) Phosphotyrosine interactome of the ErbB-receptor kinase family. *Mol. Syst. Biol.* **1**, 2005.0008.

Shah, R. and Lester, J. F. (2020) Tyrosine kinase inhibitors for the treatment of EGFR mutation-positive non-small-cell lung cancer: a clash of the generations. *Clin. Lung Cancer* **21**, e216-e228.

Shah, Z., Gohar, U. F., Jamshed, I., Mushtaq, A., Mukhtar, H., Zia-Ui-Haq, M., Toma, S. I., Manea, R., Moga, M. and Popovici, B. (2021) Podophyllotoxin: history, recent advances and future prospects. *Biomolecules* **11**, 603.

Siegel, R. L., Miller, K. D., Fuchs, H. E. and Jemal, A. (2022) Cancer statistics, 2022. *CA Cancer J. Clin.* **72**, 7-33.

Tian, X., Gu, T., Lee, M. H. and Dong, Z. (2022) Challenge and countermeasures for EGFR targeted therapy in non-small cell lung cancer. *Biochim. Biophys. Acta Rev. Cancer* **1877**, 188645.

Trott, O. and Olson, A. J. (2010) AutoDock Vina: improving the speed and accuracy of docking with a new scoring function, efficient optimization, and multithreading. *J. Comput. Chem.* **31**, 455-461.

Vasilcanu, D., Girnita, A., Girnita, L., Vasilcanu, R., Axelson, M. and Larsson, O. (2004) The cyclolignan PPP induces activation loop-specific inhibition of tyrosine phosphorylation of the insulin-like growth factor-1 receptor. Link to the phosphatidyl inositol-3 kinase/Akt apoptotic pathway. *Oncogene* **23**, 7854-7862.

Zhao, W., Cong, Y., Li, H. M., Li, S., Shen, Y., Qi, Q., Zhang, Y., Li, Y. Z. and Tang, Y. J. (2021) Challenges and potential for improving the druggability of podophyllotoxin-derived drugs in cancer chemotherapy. *Nat. Prod. Rep.* **38**, 470-488.

Zorov, D. B., Juhaszova, M. and Sollott, S. J. (2014) Mitochondrial reactive oxygen species (ROS) and ROS-induced ROS release. *Physiol. Rev.* **94**, 909-950.